Rapid Kinetics of the EPR-Active Species Formed during Initial Iron Uptake in Horse Spleen Apoferritin†

Shujun Sun and N. Dennis Chasteen*

Department of Chemistry, Parson's Hall, University of New Hampshire, Durham, New Hampshire 03824

Received June 7, 1994; Revised Manuscript Received September 28, 1994®

ABSTRACT: The molecular mechanism of oxidative deposition of iron in ferritin is incompletely understood. In this study, EPR-active species produced during ferritin reconstitution (10−50 Fe/protein) from the apoprotein, Fe^{2+}, and O_2 have been investigated using rapid-mixing freeze−quench techniques and EPR spectroscopy. Species studied include a monomeric Fe^{3+}−protein complex ($g' = 4.3$), a mixed-valent Fe^{2+}−Fe^{3+} complex ($g' = 1.87$), and a newly observed radical with axial symmetry ($g_{\|} = 2.042$, $g_{\perp} = 2.0033$), all apparent intermediates formed during the first second of iron oxidation. The monomeric Fe^{3+}−protein complex is the principal EPR-observable product of iron(II) oxidation and is produced quantitatively in the first phase of the reaction with the mixed-valent species and the radical formed at slower rates. The initial rate of formation of the monomeric complex (and the radical) is first-order in Fe^{2+} concentration, consistent with a mechanism in which iron oxidation occurs in a one-electron step(s) with H_2O_2 being the final product of O_2 reduction. A 1:1 relationship between the disappearance of the monomeric Fe^{3+}−protein complex and the formation of the mixed-valent Fe^{2+}−Fe^{3+} species was observed in the early phase of the reaction, indicating that the latter is derived from the former and not from the one-electron oxidation of a preformed Fe^{2+}−Fe^{2+} dimer. The *g*-factors and rapid EPR relaxation properties of the transient radical suggest that it is associated with an Fe^{2+} (or Fe^{3+}) center but its identity and possible functional role in iron oxidation are unknown.

Ferritin is the principal reservoir for intracellular iron in animals and plants (Theil, 1987, 1989; Andrews et al., 1992; Harrison et al., 1991). The structure of ferritin and the molecular mechanisms by which ferritin sequesters, stores, and releases iron have been the subjects of years of intensive research (Clegg et al., 1980; Harrison & Lilley, 1989). Ferritin consists of two components, a spherical protein shell of MW ~455 000 and a ferrihydrite-like mineral core. The 24mer protein shell of most mammalian ferritins consists of heteropolymer mixtures of H and L subunits of slightly different molecular weights (Arosio et al., 1978; Theil, 1989). Horse spleen ferritin typically is composed of 85% L- and 15% H-subunits assembled into a symmetric protein shell with a central cavity 80 Å in diameter (Clegg et al., 1980). Eight hydrophilic 3-fold channels lead to the interior of the protein cavity. In vitro, the iron core of ferritin can be reconstituted from apoferritin and Fe^{2+} in the presence of molecular oxygen (Harrison et al., 1967).

During iron oxidation and deposition in ferritin, Fe^{2+} is thought to bind to the outer surface of the protein and then migrates via the channels to ferroxidase sites located inside the protein shell where it is oxidized. The resulting Fe^{3+} is then translocated to nucleation sites where polynuclear Fe^{3+} cluster formation ensues. Ligands of the ferroxidase site on the H-subunit as well as the putative nucleation site have been identified by site-directed mutagenesis and X-ray crystallography (Lawson et al., 1989, 1991). However, the mechanistic details concerning Fe^{2+} migration to the ferroxidase sites, the oxidation of the Fe^{2+} at these sites, and the subsequent translocation of Fe^{3+} to nucleation sites where the iron core is laid down have not been fully elucidated.

A variety of spectroscopic techniques, including UV−vis, electron paramagnetic resonance (EPR),[1] and Mössbauer, have been employed to better understand the molecular mechanism of iron uptake by horse and human ferritins. Several intermediate species have been observed during the initial stages of ferritin formation. These species include Fe^{2+}−protein and mononuclear Fe^{3+}−protein complexes, an Fe^{2+}−Fe^{3+} mixed-valent dimer, Fe^{3+}−Fe^{3+} dimers, various sized Fe^{3+} clusters, and an Fe^{3+}−tyrosinate complex (Bauminger et al., 1989, 1991, 1993; Jacobs et al., 1989; Yang et al., 1987; Frankel et al., 1987; Rosenberg & Chasteen, 1982; Chasteen et al., 1985; Waldo & Theil, 1993; Waldo et al., 1993). EPR spectroscopy has revealed three signals upon aerobic iron(II) oxidation in ferritin. A signal at $g' = 4.3$ has been ascribed to a monomeric Fe^{3+}−protein complex (Chasteen & Theil, 1982; Rosenberg & Chasteen, 1982), while other signals at $g' = 1.87$ and $g = 2.00$ have been assigned to dimeric mixed-valent Fe^{2+}−Fe^{3+} species and protein radicals, respectively (Chasteen et al., 1985; Hanna et al., 1991b; Grady et al., 1989). The roles of these species in the overall sequence of iron oxidation and core formation are unclear, however.

Most previous kinetic measurements have been performed at reaction times of minutes to several hours. Short-lived intermediate species generated at the very early stages of ferritin formation may have already decayed away in these

† This work was supported by Grant R37 GM20194 from the National Institutes of Health.

* To whom correspondence should be addressed.

® Abstract published in *Advance ACS Abstracts,* November 15, 1994.

[1] Abbreviations: DMSO, dimethyl sulfoxide; EPPS, *N*-(2-hydroxyethyl)piperazine-*N*′-3-propanesulfonic acid; EPR, electron paramagnetic resonance; EXAFS, extended X-ray absorption fine structure; MOPS, 3-(*N*-morpholino)propanesulfonic acid; Trizma, tris(hydroxymethyl)-aminomethane.

0006-2960/94/0433-15095$04.50/0

relatively long time intervals. Also, complications arise from the onset of more than one pathway for iron oxidation as the reaction proceeds and the core develops. Therefore, in the present work, kinetic studies of the EPR-active species formed in the early stages of iron(II) oxidation were conducted by combining rapid-mixing freeze−quench techniques with EPR spectroscopy. Reaction times of milliseconds to minutes were employed. In this way, EPR-active species can be observed at the very onset of iron oxidation and their sequence of formation established. Since these types of experiments require very large quantities of protein, our initial study was carried out with the easily obtained and well-studied horse spleen protein.

The rapid-freeze−quench data reported here provide new information on the EPR-observable transient species formed during the oxidative deposition of iron in apoferritin and complement recent UV−visible experiments employing stopped-flow kinetics (Bauminger et al., 1993; Waldo et al., 1993; Waldo & Thiel, 1993; Le Brun et al., 1993). The $g' = 4.3$ mononuclear Fe^{3+}−apoferritin complex is the principal EPR-observable species initially formed in the very early stage of iron(II) oxidation followed by the $g' = 1.87$ mixed-valent Fe^{2+}−Fe^{3+} complex. The latter species is derived from the former within the first second of the reaction. Polynuclear EPR-silent Fe^{3+} species are formed later. Moreover, a new radical signal of axial symmetry has been observed and postulated to arise from a protein radical generated during the one-electron oxidation of iron(II). From its EPR relaxation properties, the radical appears to be associated with an iron center.

MATERIALS AND METHODS

Materials. Horse spleen ferritin, bovine liver catalase (EC 1.11.1.6), bovine erythrocyte superoxide dismutase (EC 1.15.1.1), and *Aspergillus niger* glucose oxidase (EC 1.1.3.4) were purchased from Boehringer Mannheim; MOPS[1] [3-(*N*-morpholino)propanesulfonic acid] was from Research Organics Inc.; α-D(+)-glucose and *N*-(2-hydroxyethyl)piperzine-*N*′-3-propanesulfonic acid (EPPS) were purchased from Sigma Chemical Co.; ferrous sulfate heptahydrate was obtained from J. T. Baker Co.; zinc sulfate heptahydrate was from Mallinckrodt Chemical Works; and terbium(III) chloride hexahydrate was from Aldrich. $^{17}O_2$ (85.2% isotopically enriched) was obtained from ICON Services and used as a 70% O_2−30% N_2 mixture. A 0.1 M stock solution of KO_2 was prepared in dimethyl sulfoxide (DMSO) containing 0.1 M dicyclohexyl-18-crown-6. Apoferritin was prepared by dialysis against 1% thioglycolic acid (TGA) and 0.15 M NaCl as described previously (Hanna et al., 1991b). The concentration of the apoferritin was measured on a Cary 219 spectrophotometer at 280 nm (Bryce & Crichton, 1971). The stock solution of apoferritin was stored in 0.05 M MOPS, pH 7.1, at 4 °C.

Freeze−Quench Experiments. All rapid-mixing experiments were performed at room temperature (22−23 °C) on a System 1000 chemical/freeze−quench apparatus manufactured by Update Instrument Inc. The temperature of the isopentane, monitored with a copper constantan thermocouple, was maintained at −130 ± 5 °C. In a typical experiment, two syringes of 2.0 and 0.5 mL volume were used. Samples of 300 μL total volume from the two syringes mixed in a 4:1 ratio were pushed through a reactor hose and the spray nozzle at a velocity of 2 cm/s into the liquid isopentane contained in a funnel to which a 5 in. long precision quartz EPR tube (3 mm i.d. and 4 mm o.d.) was attached. The small crystals formed in the isopentane reservoir were packed into the EPR tube within 1 min. The EPR tube containing the acquired sample was then disconnected from the funnel and stored in a dry ice/acetone slush bath at −77 °C; the isopentane inside the EPR tube was pumped away under vacuum. Subsequently, a 5 in. piece of open-ended quartz tubing was attached to the top of the EPR tube using a piece of heat-shrink tubing, enabling the sample tube to be used with the low-temperature EPR cryostat. Samples were stored at −126 °C for later EPR measurements.

The dead time of the instrument was determined using the standard reaction of metmyoglobin with sodium azide as previously described (Brenner et al., 1989; Ballou & Palmer, 1974). A solution of 1.0 mM metmyoglobin in 0.02 M Trizma-HCl/0.1 M KNO_3 buffer, pH 7.8, was shot against buffer or against 25 mM sodium azide in buffer. The binding of azide ion to metmyoglobin causes the conversion of the high-spin Fe^{3+} to low-spin, and therefore the disappearance of the $g \simeq 5$ signal. The apparent rate constant, k_{app} (30.6 ± 1.7 s^{-1}), obtained was close to the previously reported value of 34.0 s^{-1} (Ballou & Palmer, 1974). A dead time of 15 ± 2 ms for the instrument was determined following procedures described elsewhere (Ballou & Palmer, 1974).

Kinetic Measurements of the EPR-Active Species. In the kinetic studies, samples collected in the rapid-mixing experiments were prepared by shooting 52 μM apoferritin in 0.1 M MOPS, pH 7.1, buffer (2 mL syringe) against varying concentrations of Fe^{2+} solution (2.0−10.0 mM) in 0.01 M HCl (0.5 mL syringe) to give concentrations of 42 μM protein and 0.4, 0.8, and 2.0 mM Fe^{2+} in the final solution. Zinc inhibition experiments were carried out by incubating 52 μM apoferritin in 0.1 M MOPS, pH 7.1, with 1.25 mM zinc(II) for about 2 h. The Zn^{2+}−protein solution was then shot against a 10.0 mM Fe^{2+} solution in 0.01 M HCl. Tb^{3+} inhibition experiments were performed by manually mixing 300 μL of 42 μM apoferritin solution containing 24 Tb^{3+} (as $TbCl_3 \cdot 6H_2O$) per protein with 1.2 μL of 0.1 M $FeSO_4$ to give a Fe^{2+}:protein ratio of 9.6:1. Samples were allowed to age 10−90 s before being frozen in a dry ice/acetone slush. Oxygen uptake experiments were performed with a Clark oxygen microelectrode having a 90% response time of 6 s as previously described (Sun & Chasteen, 1992). The initial rate of O_2 uptake was obtained from the linear term in a cubic least-squares fit to the O_2 concentration−time curve (Waldo & Theil, 1993). At the concentrations of protein (42 μM) and Fe^{2+} (0.4 mM) employed, the reaction was complete in approximately 40 s.

Relationship between the Monomeric and Dimeric Complexes. Experiments designed to study the relationship between the mononuclear $g' = 4.3$ Fe^{3+}−apoferritin complex and the dimeric $g' = 1.87$ Fe^{2+}−Fe^{3+} species were performed under strictly anaerobic conditions. A solution of 42 μM ferritin containing 6 Fe^{3+}/protein, 61.5 mM glucose, and 0.75 mg/mL catalase in 0.1 M MOPS buffer, pH 7.1, was first deaerated by passing prepurified moistened argon gas over the stirred protein solution for 1 h; 150 units/mL glucose oxidase was then introduced to the deaerated protein sample by a syringe to remove trace amounts of O_2. The deoxygenated ferritin solution was then shot against a predeaerated

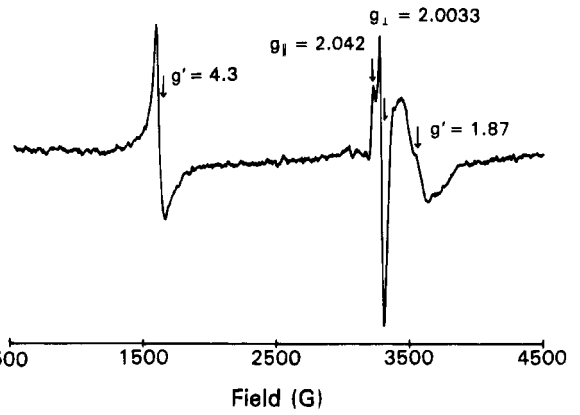

FIGURE 1: EPR spectrum of partially oxidized ferritin at an Fe:protein ratio of 48:1. Conditions: [apoferritin] = 42 μM, $[Fe^{2+}]_0$ = 2.0 mM, $[O_2]_0$ = 0.25 mM, 80 mM MOPS, pH 7.1, reaction temperature = 23 °C, reaction time = 5.4 s. Instrument settings: modulation amplitude = 10 G at 100 kHz; receiver gain = 8000; time constant = 1 s; frequency = 9.360 GHz; scan rate = 4000 G/8 min; microwave power = 0.5 mW; T = 7.2 K.

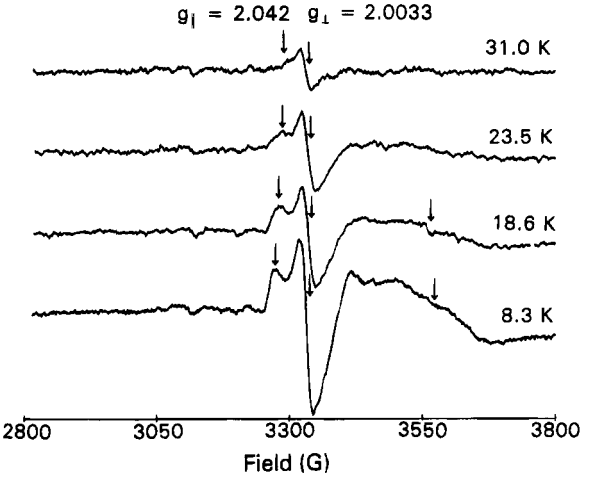

FIGURE 2: Temperature dependence of the axially symmetric radical signal. Conditions: [apoferritin] = 42 μM, $[Fe^{2+}]_0$ = 2.0 mM, $[O_2]_0$ = 0.25 mM, 80 mM MOPS, pH 7.1, reaction temperature = 23 °C, reaction time = 5.4 s. Instrument settings: same as Figure 1 except for a scan rate of 400 G/8 min.

10.0 mM Fe^{2+} solution, pH 2.0, at various times, or against deaerated 0.01 M HCl as a control.

EPR Measurements. EPR spectra were recorded on a Varian E-4 spectrometer at 77 K using a quartz dewar insert in a TE_{102} cavity or on a Varian E-9 spectrometer with a TE_{104} rectangular dual cavity at liquid helium temperatures using an Air Products Helitran flow cryostat and a Cryo Industries of America transfer line. Temperatures were measured before and after each spectrum with a carbon glass resistor sensor (TRI Research). The EPR spectrometers were interfaced to an ISA standard Intel-based 80486 computer using data acquisition hardware. Data acquisition and manipulation was performed with EPRWare software from Scientific Software Services of Bloomington, IL.

Varian strong pitch (g = 2.0028) and a standard Mn^{2+} in CaO sample (g_0 = 2.0011, a_0 = 86.23 G) were employed to calculate the g-factors of the EPR signals and to check the field sweep calibration. Spin concentrations were determined using 0.36 mM differic transferrin solution in 0.1 M Hepes/0.01 M NaH_2CO_3, pH 7.5, as a standard for the g' = 4.3 signal and 0.5 mM $Cu(NO_3)_2$ in 25% glycerol, pH 2.0, for the radical and the mixed-valent signals. The standards were frozen by rapid-freezing as for the unknowns. Double integrals of the copper(II) and diferric transferrin standards agreed within 3.1% after correcting for their metal concentrations, g-factors, and the equal populations of the three doublets of the $S = {}^5/_2$ spin manifold of states of the Fe^{3+}. The value of the double integral of the mixed-valent species was obtained by subtracting the double integral of the radical signal from the total integral of the two signals.

RESULTS

EPR-Active Species. Iron EPR signals at g' = 4.3 and g' = 1.87 and a radical signal of axial symmetry, $g_{\parallel}$ = 2.042 and $g_{\perp}$ = 2.0033, are observed in frozen solution after rapid mixing of Fe^{2+} with an aerobic apoferritin solution (Figure 1). The incubation time was 5.4 s, the sample was quick-frozen at −130 °C, and the spectrum was recorded at 7.3 K. While the mononuclear Fe^{3+}−apoferritin EPR signal at g' = 4.3 and the dimeric Fe^{2+}−Fe^{3+} signal at g' = 1.87 have been observed previously (Rosenberg & Chasteen, 1982; Chasteen et al., 1985; Hanna et al., 1991b), the axially symmetric radical signal has not been seen before.

Characterization of the Radical Signal. Figure 2 illustrates the temperature-dependent properties of the radical signal. The radical signal rapidly decreases in amplitude with increasing temperature and broadens into the base line (Figure 2). The axial signal is nearly gone at 31 K, and a weak isotropic signal at g = 2.0078 from a second radical is observable (Figure 2, top trace). Only the isotropic signal remains at 77 K (data not shown); the axial signal is absent at the higher temperature presumably due to rapid spin−lattice relaxation. A nonlinear regression fit of eq 1 of Styring and Rutherford (1988) to the microwave power saturation curve (EPR amplitude *vs* power) at 4.3 K gave a value for the power at half-saturation of $P_{1/2} = 0.21 \pm 0.02$ mW and a homogeneity parameter of $b = 0.94 \pm 0.02$. The temperature dependencies of the $g_{\parallel}$ and $g_{\perp}$ components of the axial signal are illustrated in Figure 3 and approximate the Curie law below 25 K.

The line shape of the axial radical signal is independent of reaction time, pH, and buffer as well as the initial oxygen concentration. However, the intensity of the signal decreases by about 50% upon increasing the pH of the kinetics experiment from 7.1 to 9.5, implying that the radical is not a product of autoxidation of Fe^{2+} which is favored by higher pH (Sun et al., 1993; Levi et al., 1989). As the initial oxygen concentration is increased from 0.25 to 1.27 mM, the axial EPR signal measured at 8.3 K increases by 40%. In the same experiment, the isotropic radical signal at g = 2.0078 measured at 77 K increased by only 11%. However, because the isotropic signal appeared to be the same as that previously attributed to radical damage to the protein from Fenton chemistry (Grady et al., 1989), it was not investigated further.

Figure 4 shows the effect of the initial iron(II) concentration on the EPR amplitudes of the mixed-valent signal and the axial radical signal. It is evident that the axial radical signal is not associated with the mixed-valent Fe^{2+}−Fe^{3+} species since the two signals change disproportionately with initial Fe^{2+} concentration.

The line shape and g-factors of the axially symmetric radical signal (reaction time of 5.4 s) were found to be

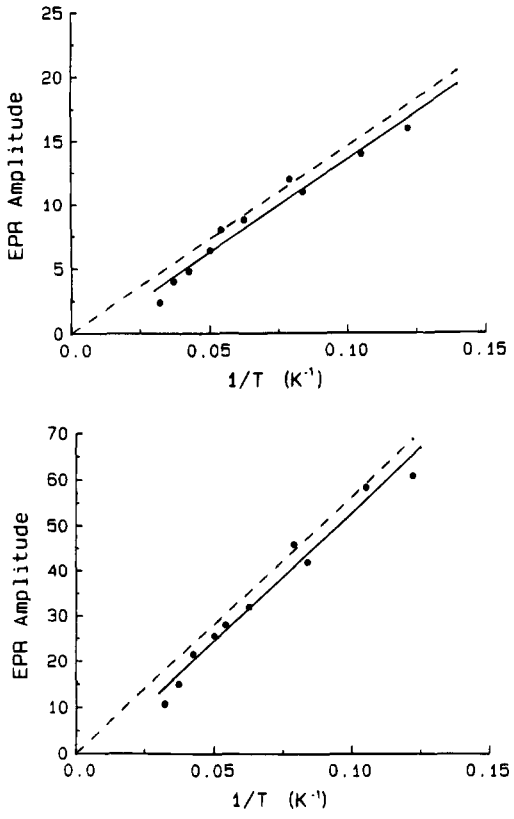

FIGURE 3: Temperature dependence of the radical signal at $g_{\parallel} = 2.042$ (lower panel) and $g_{\perp} = 2.0033$ (upper panel). Conditions are the same as described in Figure 2.

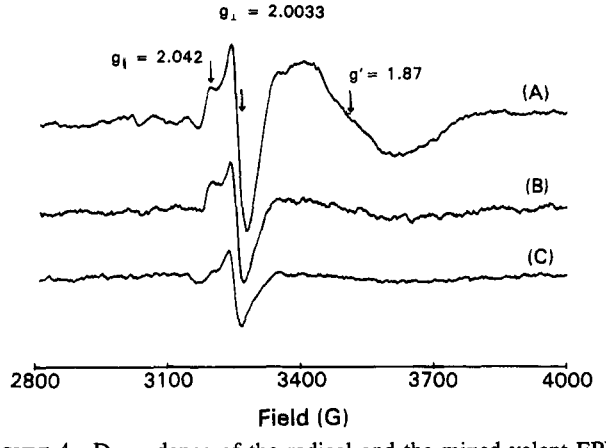

FIGURE 4: Dependence of the radical and the mixed-valent EPR signals on the initial Fe^{2+} concentrations. Conditions: [apoferritin] = 42 μM, $[O_2]_0$ = 0.25 mM in 80 mM MOPS buffer, pH 7.1, $[Fe^{2+}]_0$ = 2.0 mM (Fe/protein = 47.6) (A), 0.8 mM (Fe/protein = 19.0) (B), and 0.4 mM (Fe/protein = 9.5) (C), reaction temperature = 23 °C, reaction time = 5.4 s. Instrument settings as listed in Figure 1.

different from those of the superoxide radical (Knowles et al., 1969), and unlike the radical previously observed at longer reaction times of 5 min (Grady et al., 1989). No ^{17}O coupling in the EPR spectrum was observed when $^{17}O_2$ was used as the oxidant (data not shown), suggesting that the EPR signal is not due to an oxy or peroxyl radical [*cf.* Nelson and Cowling (1990) and Nelson et al. (1994)]. Nor does the axially symmetric signal derive from hydroxyl radical damage to the protein since rapid-mixing of H_2O_2 with the Fe^{2+}–apoprotein complex in the absence of O_2 produces a fine structure spectrum instead (data not shown). That the

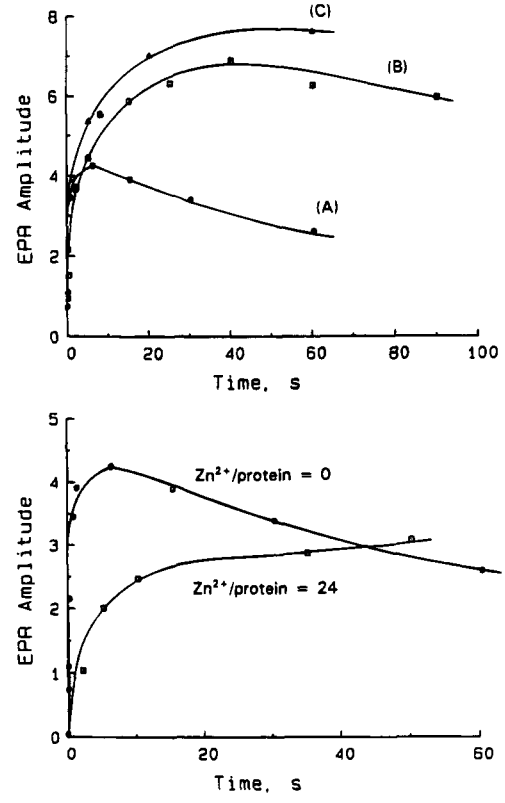

FIGURE 5: Upper panel: EPR amplitude versus time for the mononuclear Fe^{3+}–protein signal at $g' = 4.3$. Conditions: [apoferritin] = 42 μM, $[O_2]_0$ = 0.25 mM, in 80 mM MOPS, pH 7.1, reaction temperature = 23 °C; $[Fe^{2+}]_0$ = 2.0 mM (curve A), 0.8 mM (curve B), and 0.4 mM (curve C). Lower panel: Zn^{2+} inhibition on the formation of the $g' = 4.3$ signal. Conditions are the same for curve A of the upper panel. Instrument settings are the same as in Figure 1.

observed axial radical does not derive from hydroxyl radical is also supported by the observation that neither superoxide dismutase nor catalase has any significant effect on its formation.

Kinetics of Formation and Zn^{2+} Inhibition of the EPR-Active Species. The kinetics of formation of the $g' = 4.3$ EPR species at different initial Fe^{2+} concentrations are shown in the upper panel of Figure 5. In the presence of excess ferrous ion ($[Fe^{2+}]_0$ = 2.0 mM) over the dissolved dioxygen concentration of about 0.25 mM, the $g' = 4.3$ EPR signal is formed within milliseconds, reaches a maximum in around 10 s, and then rapidly decays (Figure 5, trace A). At a lower concentration of ferrous ion ($[Fe^{2+}]_0$ = 0.80 mM), the maximum in EPR amplitude was observed at a reaction time of about 40 s followed by a slower decay (Figure 5, trace B). A hyperbolic relation of the EPR amplitude versus time was observed at $[Fe^{2+}]_0$ = 0.40 mM (Figure 5, trace C) with no appreciable decay in the signal. In this case, no remaining Fe^{2+} was present in solution since sufficient O_2 was present to consume all the added Fe^{2+} within 40 s of initiating the reaction.

The initial rate of formation of the monomeric Fe^{3+}–protein $g' = 4.3$ complex in the first seconds of the iron(II) oxidation reaction follows first-order kinetics in Fe^{2+} concentration as determined here (graph not shown) and in protein concentration as determined previously (Sun & Chasteen, 1992), *viz.*

$$d[Fe^{3+}\text{–protein}]/dt = k_{app}[Fe^{2+}][\text{apoferritin}] \quad (1)$$

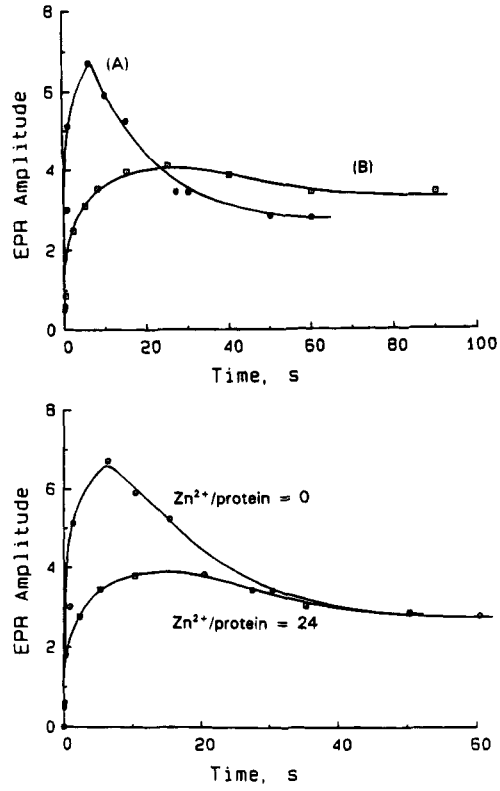

FIGURE 6: Upper panel: EPR amplitude versus time for the mixed-valent signal at $g' = 1.87$. Conditions: [apoferritin] = 42 μM, $[O_2]_0 = 0.25$ mM, in 80 mM MOPS, pH 7.1, reaction temperature = 23 °C, $[Fe^{2+}]_0 = 2.0$ mM (curve A) and 0.8 mM (curve B). Lower panel: Zn^{2+} inhibition on the formation of the $g' = 1.87$ mixed-valent signal. Conditions are the same as listed for curve A in the upper panel. Instrument settings are the same as in Figure 1 except that microwave power = 90 mW.

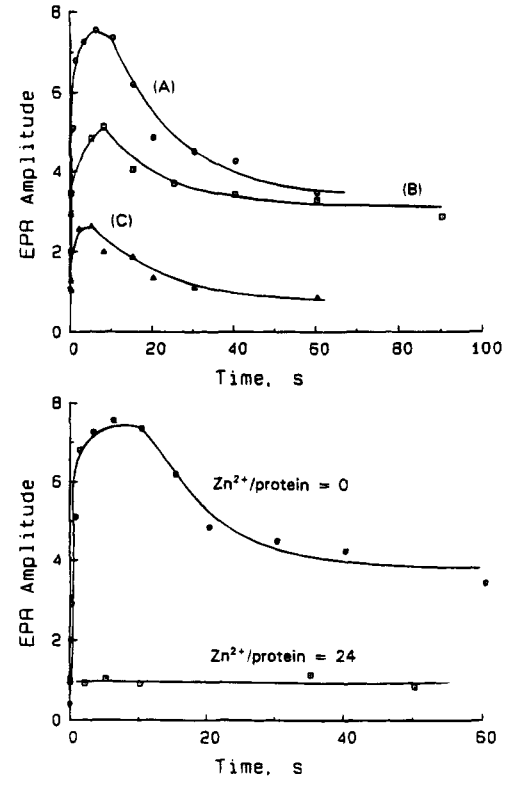

FIGURE 7: Upper panel: EPR amplitude versus time for the radical signal at $g = 2.0033$. Lower panel: Zn^{2+} inhibition on the formation of the radical signal. Experimental conditions and instrument settings are as listed in Figure 5.

An apparent second-order rate constant of $k_{app} = 1.4 \pm 0.2$ mM^{-1} s^{-1} at an O_2 concentration of 0.25 mM was obtained. At 0.40 mM Fe^{2+}, the initial rate of formation of the $g' = 4.3$ complex is 0.016 ± 0.004 mM/s, which is close to the value of 0.019 ± 0.001 mM/s for oxygen consumption measured by electrode oximetry under the same conditions (Materials and Methods).

The lower panel of Figure 5 illustrates the Zn^{2+} inhibition of the $g' = 4.3$ EPR signal at an Fe^{2+} concentration of 2.0 mM (47.6 Fe/protein). A total of 24 Zn^{2+} per protein molecule was added prior to the Fe^{2+}. The initial rate of formation of the $g' = 4.3$ signal is decreased 10-fold by the presence of Zn^{2+}, in accord with the known Zn^{2+} inhibition of the protein-catalyzed oxidation of Fe^{2+} (Sun & Chasteen, 1992; Sun et al., 1993; Treffry & Harrison, 1984; Macara et al., 1973). The addition of 24 Tb^{3+} per protein molecule prior to manually adding Fe^{2+} (Materials and Methods) nearly completely blocks formation of the $g' = 4.3$ complex, the maximum amplitude of the signal being attenuated by 85% compared to a control sample prepared in the same way without Tb^{3+}. Tb^{3+} has been shown from competition experiments to displace the $g' = 4.3$ Fe^{3+} from its (their) site(s) on the protein (Rosenberg & Chasteen, 1982; Treffry et al., 1993).

Figure 6 shows the EPR amplitude versus time for the mixed-valent ($g' = 1.87$) signal at two initial iron(II) concentrations of 2.0 mM (trace A) and 0.80 mM (trace B), as well as the effect of Zn^{2+} on this signal. The $g' = 1.87$ signal is not observed above the spectral noise when 0.4 mM Fe^{2+} is employed. The time course of the EPR amplitude is quite distinctive for each initial Fe^{2+} concentration (Figure 6, upper panel). The same trends are observed as for the $g' = 4.3$ signal, that is, an initial burst in EPR amplitude followed by an immediate rapid decrease in the signal at the higher added Fe^{2+} concentration (Figure 6, trace A). At the lower Fe^{2+} concentration, slow growth in EPR intensity is observed followed by a slower decay of the signal (Figure 6, trace B). In addition, the $g' = 1.87$ mixed-valent Fe^{2+}–Fe^{3+} signal does not decay to zero since there is insufficient O_2 in the solution to consume all of the Fe^{2+} present (traces A and B). The rate of formation of the $g' = 1.87$ signal is also less in the presence of Zn^{2+} (Figure 6, lower panel) as observed for the $g' = 4.3$ signal.

Figure 7 (upper panel) illustrates the time dependence of the radical signal at various Fe^{2+} concentrations. The radical signal increases rapidly with time, reaches a maxima at about 10 s, and then decays. The initial rate follows first-order kinetics in Fe^{2+} concentration (graph not shown). The apparent second-order rate constant for radical formation is about 0.4 mM^{-1} s^{-1} (first-order each in Fe^{2+} and protein concentrations), a value approximately one-fourth of that observed for the formation of the monomeric Fe^{3+}–protein complex noted above (eq 1). Zinc greatly inhibits the formation of the axially symmetric radical signal when 24 Zn^{2+}/protein are added prior to adding Fe^{2+} (Figure 7, lower panel).

Figure 8 compares the formation of the mononuclear $g' = 4.3$ complex (curve A), the mixed-valent $g' = 1.87$ complex (curve B), and the radical (curve C) in the early phase of the reaction when 2.0 mM Fe^{2+} is employed. The $g' = 4.3$ species is formed first followed by the mixed-valent and the radical species. One radical is observed per

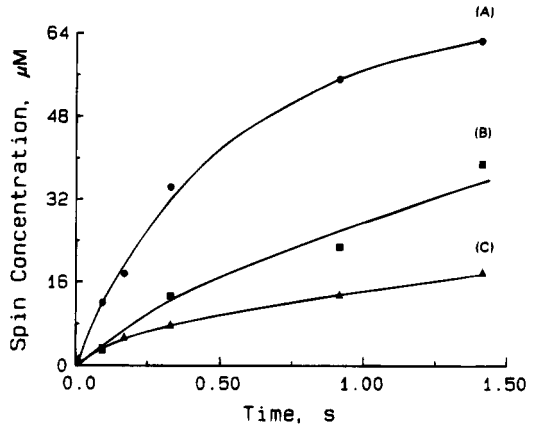

FIGURE 8: Kinetics of formation of the three EPR-active species at the early stage of iron(II) oxidation. Conditions: [apoferritin] = 42 μM, $[O_2]_0$ = 0.25 mM, $[Fe^{2+}]_0$ = 2.0 mM, in 80 mM MOPS, pH 7.1, reaction temperature = 23 °C. (A) g' = 4.3; (B) g' = 1.87; and (C) g = 2.00. Instrument settings are the same as in Figure 1.

Table 1: Maximum Spin Concentrations of the Three EPR-Active Species at Different Initial Fe^{2+} Concentrations[a,b,c]

	$[Fe^{2+}]_0$, mM		
	2.00	0.80	0.40
mononuclear $[Fe^{3+}]$, μM (g' = 4.3)	70	100	120
mixed-valent $[Fe^{2+}-Fe^{3+}]$, μM (g' = 1.87)	51	23	~0
[axial radical], μM ($g_{\parallel}$ = 2.042, $g_{\perp}$ = 2.0033)	20	10	8

[a] Conditions: [apoferritin] = 42 μM, $[O_2]_0$ = 0.25 mM in 80 mM MOPS, pH 7.1, at 23 °C. [b] The field ranges for the double integrations of the g' = 4.3, g' = 1.87, and g = 2.0033 signals are approximately 1200–2300, 3020–4100, and 3020–3360 G, respectively. EPR microwave frequency is 9.36 GHz. [c] Estimated errors in spin concentrations are ±15%.

approximately six Fe^{3+} produced (as the sum of monomeric Fe^{3+} and mixed-valent $Fe^{2+}-Fe^{3+}$ species). Table 1 summarizes the maximum spin concentrations of the three S = $^1/_2$ EPR-active species at various initial Fe^{2+} concentrations.

Relationship between the Mononuclear Fe^{3+}–Protein and Dimeric $Fe^{2+}-Fe^{3+}$ Complexes. Rapid-mixing of anaerobic ferritin samples containing 6 Fe^{3+} per protein molecule with an anaerobic 2 mM Fe^{2+} solution in 0.01 M HCl led to the appearance of the g' = 1.87 $Fe^{2+}-Fe^{3+}$ signal and the concomitant disappearance of the g' = 4.3 signal (Figure 9, spectra B and C) compared to a control experiment in which the Fe^{3+}–apoferritin sample was shot against 0.01 M HCl alone (Figure 9, spectrum A). Under the experimental conditions, the interconversion between the two species took place within a second. The $Fe^{2+}-Fe^{3+}$ dimer spin concentrations of 0.020 and 0.040 mM determined at reaction times of 170 and 330 ms are very close to the corresponding decrease in the Fe^{3+}–protein monomer concentrations of 0.024 and 0.050 mM at these times, respectively, a result indicating that the former complex is quantitatively derived from the latter.

DISCUSSION

The EPR-active species observed in the present work are three intermediates produced during the oxidative deposition of iron in apoferritin (Figure 1). Due to the rapid onset of iron clusters, the EPR-detectable iron–protein complexes account for only a percentage of the total Fe^{3+} present in

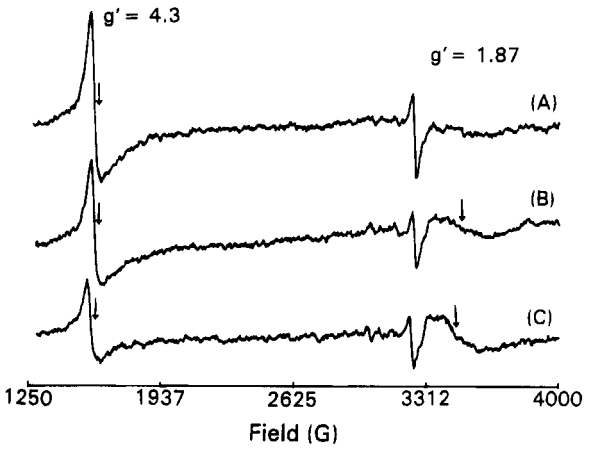

FIGURE 9: EPR spectra of ferritin containing 6 Fe^{3+} per protein in the absence (spectrum A) and presence (spectra B and C) of 48 Fe^{2+} per protein molecule. Conditions: [apoferritin] = 42 μM, $[Fe^{3+}]$ = 0.25 mM, $[Fe^{2+}]$ = 0 (spectrum A) and 2.0 mM (spectra B and C), [glucose] = 49.2 mM, [glucose oxidase] = 0.58 mg/mL, [catalase] = 380 units/mL, in 80 mM MOPS, pH 7.15, reaction temperature = 23 °C. Aging time after anaerobically mixing Fe^{2+} with the protein solution: 0.17 s (spectrum B) and 0.33 s (spectrum C). Instrument settings are equivalent with those described in Figure 1 except for T = 11.3 K.

ferritin depending upon the Fe^{3+}/protein ratio and the reaction time. For example, the largest g' = 4.3 spin concentration was observed with $[Fe^{2+}]_0$ = 0.40 mM at a reaction time of about 50 s and accounted for about 30% of the total Fe^{3+} in the protein (Table 1 and Figure 5). This value is comparable to the 50% Fe^{3+} monomers observed by Mössbauer spectroscopy at a reaction time of 1 min and under similar solution conditions as employed here [see Table II of Bauminger et al. (1989)].

The g' = 4.3 signal is observable within 50 ms after initiation of iron oxidation (Figure 8, curve A). The initial burst in intensity of the EPR signal implies that much of the Fe^{3+} produced at the very beginning of the oxidation reaction is in the form of the monomeric Fe^{3+}–protein complex, in agreement with previously reported titration and spin quantification results (Rosenberg & Chasteen, 1982; Hanna et al., 1991b). The observation that the monomeric complex is formed at essentially the same rate as oxygen is consumed (0.016 *vs* 0.019 mM/s) implies a 1:1 reaction stoichiometry. The O_2^- produced may then dismutate to $^1/_2O_2$ and $^1/_2H_2O_2$, to give the observed overall reaction stoichiometry of $2Fe^{2+}/O_2$ with hydrogen peroxide being the final product of dioxygen reduction (Xu & Chasteen, 1991). Furthermore, the 1:1 stoichiometry and the first-order kinetics in monomeric Fe^{3+} complex formation are in accord with previous kinetics and Mössbauer data suggesting that iron oxidation occurs in one-electron transfer steps (Sun & Chasteen, 1992; Sun et al., 1993; Bauminger et al., 1989). A similar first-order dependence on Fe^{2+} concentration has been reported for iron oxidation in bacterioferritin as measured by stopped-flow kinetics (Le Brun et al., 1993).

Monomeric Fe^{3+}–protein complexes have been observed at different reaction times in a number of earlier studies of horse spleen apoferritin using UV difference spectroscopy (Treffry & Harrison, 1984), EXAFS (Yang et al., 1987), and Mössbauer spectroscopy (Bauminger et al., 1989). A potential binding site for g' = 4.3 monomeric Fe^{3+} situated in or near the 3-fold channels has been suggested by EPR, ESEEM, and ENDOR measurements on the horse

spleen protein and by UV and Mössbauer spectroscopy on recombinant human ferritins and mutants (Treffrey et al., 1993; Wardeska et al., 1986; Stefanini et al., 1989; Hanna et al., 1991a; Gerfen et al., 1991). The Fe^{3+}−tyrosinate complex detected in recombinant bullfrog red cell H-chain ferritin by UV and resonance Raman spectroscopies has been attributed to a rapidly formed monomeric Fe^{3+} complex (Waldo et al., 1993), but more recent data raise the possibility of an oligonuclear species (Waldo & Theil, 1993). Mössbauer spectroscopic studies have also revealed an Fe^{3+}−protein monomer in recombinant H- and L-chain human ferritins, mutant 222 (putative ferroxidase site mutated), as well as mutant A2 (putative nucleation site mutated) (Bauminger et al., 1991). Thus, the binding sites for monomeric Fe^{3+} are not subunit-specific and cannot be exclusively at the ferroxidase site or the nucleation site on the human H-subunit (Bauminger et al., 1991). It seems likely that there is more than one type of monomeric $g' = 4.3$ Fe^{3+} binding site on the ferritins, the occupancy of which depends on the conditions of the experiment. In the present kinetics study, we are observing the principal $g' = 4.3$ monomeric Fe^{3+}−protein complex formed before significant amounts of oligonuclear and other monomeric species are generated. The $g' = 4.3$ complex observed here perhaps arises from rapid migration of Fe^{3+} to the 3-fold channels following Fe^{2+} oxidation at the putative dimeric iron ferroxidase site (Treffry et al., 1993), perhaps from the reported Fe^{3+}−tyrosinate complex (Waldo et al., 1993) since the latter is formed at a rate comparable to that observed here, or perhaps from some other site yet to be identified. It is difficult to assign the binding site for this initial monomeric Fe^{3+}−protein complex with certainty in the absence of data on site-directed mutants.

Previous studies have suggested that the $g' = 1.87$ mixed-valent complex is a transient Fe^{2+}−Fe^{3+} species observed only in the presence of excess Fe^{2+} (Chasteen et al., 1985), a result confirmed by the kinetics experiments reported here. During the reaction, its concentration never exceeds a few percent of the total iron in the sample (Table 1), accounting for the fact that it has never been observed by Mössbauer spectroscopy (Bauminger et al., 1989, 1993). When there is sufficient O_2 in the solution to oxidize all of the Fe^{2+} present, the mixed-valent species does not accumulate in sufficient amounts to be observed in the EPR spectrum. Its low concentration does not preclude it from having a role in core formation, however. The rapid one-electron oxidation of a transient mixed-valent dimer may provide a pathway for formation of the Fe^{3+}−Fe^{3+} dimer seen by Mössbauer spectroscopy (Bauminger et al., 1989).

The 1:1 conversion of the solitary Fe^{3+} complex to the mixed-valent complex upon addition of Fe^{2+} (Figure 9) is consistent with the kinetics experiments of Figure 5 (upper panel) showing that the maximum $g' = 4.3$ signal decreases with increasing Fe^{2+} concentration. Either the Fe^{2+} binds at the site on the protein where the solitary Fe^{3+} binds or, alternatively, the Fe^{2+}−Fe^{3+} complex derives its Fe^{3+} from the mononuclear Fe^{3+}−protein site but is formed elsewhere. Either scenario would give the observed 1:1 stoichiometry. At longer reaction times, some mixed-valent species may well derive Fe^{3+} from oligonuclear and polynuclear Fe^{3+} species formed later in the reaction as previously suggested (Hanna et al., 1991b). Electron transfer between ferrous and ferric ions in ferritin has been demonstrated by Mössbauer spectroscopy and may also be important in forming mixed-valent species (Jacobs et al., 1989).

Zn^{2+} blocks the initial burst in $g' = 4.3$ Fe^{3+}−protein complex formation (Figure 5, lower panel), presumably by binding at the ferroxidase site on the H-subunit or preventing Fe^{2+} from migrating to this site, thus reducing the initial rate of Fe^{3+} formation. Zn^{2+} inhibition of the formation of the mixed-valent Fe^{2+}−Fe^{3+} species (Figure 6, lower panel; Hanna et al., 1991b) probably occurs by the same mechanism. Tb^{3+} behaves similarly to Zn^{2+} but is a more potent inhibitor of $g' = 4.3$ complex formation. Multiple binding sites for Zn^{2+} and Tb^{3+} on the L-subunit of the horse spleen protein have been identified by X-ray crystallography (Harrison et al., 1985, 1986), anyone of which may influence iron oxidation and core formation.

The fact that the maximum intensity of the radical signal increases with increasing added Fe^{2+} (Figure 4), and is not detectable at higher temperature due to rapid spin relaxation, suggests that the radical is probably associated with a ferrous (or ferric) ion. Similar properties have been reported for other radicals in the vicinity of Fe^{2+}, for example, the ubisemiquinone radicals in the bacterial photosynthetic reaction center (Butler et al., 1984) and the compound I radical of cytochrome *c* peroxidase (Scholes et al., 1989). The compound I radical has *g*-factors similar to those of the axial radical and has been identified as a tryptophan-centered radical (Hori & Yonetani, 1985; Scholes et al., 1989; Fishel et al., 1991). Trp-93 (human H-chain sequence) is the only tryptophan residue found in mammalian ferritins (Andrews et al., 1992); however, it cannot be the source of the axial radical signal since the human H-chain mutant K86Q,W93F also displays the axial signal (Arosio, Santambrogio, and Chasteen, unpublished data). The axial EPR spectrum is unlike those of known tyrosyl radicals in proteins (*e.g.*, Hoganson & Babcock, 1992); however, on the basis of the present data alone, tyrosine cannot be precluded as the site of radical production. A cysteine- or histidine-centered radical is also a possibility. Further work with recombinant ferritins and site-directed mutants will be needed before the radical can be identified and its functionality established with certainty.

In summary, the monomeric Fe^{3+}−protein complex is the first EPR-detectable intermediate Fe^{3+} species formed during iron oxidation in horse spleen ferritin. In the early phase of the reaction, the $g' = 1.87$ mixed-valent Fe^{2+}−Fe^{3+} species is quantitatively produced from the monomeric Fe^{3+} complex. The axially symmetric radical is formed at about the same time and is probably associated with a ferric or ferrous ion center. It may be either a nitrogen-centered radical (a histidine), an oxygen-centered radical (a tyrosine), or a sulfur-centered radical (methionine or cysteine). The radical may have a functional role in iron oxidation, perhaps in storing oxidizing equivalents on the protein for subsequent oxidation of Fe^{2+}. Such redox centers have been observed previously with horse spleen apoferritin (Watt et al., 1992).

ACKNOWLEDGMENT

We thank Mr. John K. Grady for performing the ^{17}O experiment, Ms. Yu Chen Barrett for measuring the O_2 uptake kinetics, and Dr. Mark J. Nelson for helpful advice on handling the $^{17}O_2$.

REFERENCES

Andrews, S. C., Arosio, P., Bottke, W., Briat, J.-F., von Darl, M., Harrison, P. M., Laulhère, J.-P., Levi, S., Lobreaux, S., & Yewdall, S. J. (1992) *J. Inorg. Biochem. 47*, 161−174.

Arosio, P., Adelman, T. G., & Drysdale, J. W. (1978) *J. Biol. Chem. 253*, 4451−4458.

Ballou, D. P., & Palmer, G. A. (1974) *Anal. Chem. 46*, 1248−1253.

Bauminger, E. R., Harrison, P. M., Nowik, I., & Treffry, A. (1989) *Biochemistry 28*, 5486−5493.

Bauminger, E. R., Harrison, P. M., Hechel, D., Nowik, I., & Treffry, A. (1991) *Biochim. Biophys. Acta 1118*, 48−58.

Bauminger, E. R., Harrison, P. M., Hechel, D., Hodson, N. W., Nowik, I., & Treffry, A., & Yewdall, S. J. (1993) *Biochem. J. 296*, 709−719.

Brenner, M. C., Murray, C. J., & Klinman, J. P. (1989) *Biochemistry 28*, 4656−4664.

Bryce, C. J. A., & Crichton, R. R. (1971) *J. Biol. Chem. 246*, 4198−4205.

Butler, W. F., Calvo, R., Fredkin, D. R., Isaacson, R. A., Okamura, M. Y., & Feher, G. (1984) *Biophys. J. 45*, 947−973.

Chasteen, N. D., & Theil, E. C. (1982) *J. Biol. Chem. 257*, 7672−7677.

Chasteen, N. D.,, Antanaitis, B. C., & Aisen, P. (1985) *J. Biol. Chem. 260*, 2926−2929.

Clegg, G. A., Fitton, J. E., Harrison, P. M., & Treffry, A. (1980) *Prog. Biophys. Mol. Biol. 36*, 1−34.

Fishel, L. A., Farnum, M. F., Mauro, J. M., Miller, M. A., Kraut, J., Liu, Y., Tan, X., & Scholes, C. P. (1991) *Biochemistry 30*, 1986−1996.

Frankel, R. B., Papaefthymiou, G. C., & Watt, G. D. (1987) *Hyperfine Interact. 33*, 233−240.

Gerfen, G. J., Hanna, P. M., Chasteen, N. D., & Singel, D. J. (1991) *J. Am. Chem. Soc. 113*, 9513−9519.

Grady, J. K., Chen, Y., Chasteen, N. D., & Harris, D. C. (1989) *J. Biol. Chem. 264*, 20224−20229.

Hanna, P. M., Chasteen, N. D., Rottman, G. A., & Aisen, P. (1991a) *Biochemistry 30*, 9210−9216.

Hanna, P. M., Chen, Y., & Chasteen, N. D. (1991b) *J. Biol. Chem. 266*, 886−893.

Harrison, P. M., & Lilley, T. H. (1989) in *Iron Carrier and Iron Protein* (Loehr, T. M., Ed.) pp 123−239, VCH Publishers, Weinheim, Germany.

Harrison, P. M., Fischback, F. A., Hoy, T. G., & Haggis, G. H. (1967) *Nature 216*, 1188−1190.

Harrison, P. M., White, J. L., Smith, J. M. A., Farrants, G. W., Ford, G. C., Rice, D. W., Addison, J. M., & Treffry, A. (1985) in *Proteins of Iron Storage and Transport* (Spik, G., Montreuil, J., Crichton, R. R., & Mazurier, J., Eds.) pp 67−79, Elsevier Science Publishers, Amsterdam.

Harrison, P. M., Ford, G. C., Rice, D. W., Smith, J. M. A., Treffry, A., & White, J. L. (1986) in *Frontiers in Bioinorganic Chemistry* (Xavier, A., Ed.) p 268, VCH Verlagsgesellschaft, Weinheim, Germany.

Harrison, P. M., Andrews, S. C., Artymiuk, P. J., Ford, G. C., Guest, J. R., Hirzmann, J., Lawson, D. M., Livingstone, J. C., Smith, J. M. A., Treffry, A., & Yewdall, S. J. (1991) *Adv. Inorg. Chem. 36*, 449−486.

Hoganson, C. W., & Babcock, G. T. (1992) *Biochemistry 31*, 11874−11880.

Hori, H., & Yonetani (1985) *J. Biol. Chem. 260*, 349−355.

Jacobs, D., Watt, G. D., Frankel, R. B., & Papaefthymiou, G. C. (1989) *Biochemistry 28*, 9216−9221.

Knowles, P. F., Gibson, J. F., Pick, F. M., & Bray, R. C. (1969) *Biochem. J. 111*, 53−58.

Lawson, D. M., Treffry, A., Artymiuk, P. J., Harrison, P. M., Yewdall, S. J., Luzzago, A., Cesareni, G., Levi, S., & Arosio, P. (1989) *FEBS Lett. 254*, 207−210.

Lawson, D. M., Artymuik, P. J., Yewdall, S. J., Smith, J. M. A., Livingstone, J. C., Treffry, A., Luzzago, A., Levi, S., Arosio, P., Cesareni, G., Thomas, C. D., Shaw, W. V., & Harrison, P. M. (1991) *Nature 349*, 541−544.

Le Brun, N. E., Wilson, M. T., Andrews, S. C., Guest, J. R., Harrison, P. M., Thomson, A. J., & Moore, G. R. (1993) *FEBS Lett. 333*, 197−202.

Lee, M., Arosio, P., Levi, S., & Chasteen, N. D. (1994) *Biochemistry 33*, 3679−3687.

Levi, S., Salfeld, J., Franceschinelli, F., Cozzi, A., Dorner, M. H., & Arosio, P. (1989) *Biochemistry 28*, 5179−5184.

Macara, J. G., Hoy, T. G., & Harrison, P. M. (1973) *Biochem. J. 135*, 785−789.

Nelson, M. J., & Cowling, R. A. (1990) *J. Am. Chem. Soc. 112*, 2820−2821.

Nelson, J. J., Cowling, R. A., & Seitz, S. P. (1994) *Biochemistry 33*, 4966−4973.

Rosenberg, L. P., & Chasteen, N. D. (1982) in *Biochemistry & Physiology of iron* (Saltman, P., & Hegenauer, J., Eds.) pp 405−407, Elsevier Biomedical, New York.

Scholes, C. P., Liu, Y., Fishel, L. F., Farnum, M. F., Mauro, J. M., & Kraut, J. (1989) *Isr. J. Chem. 29*, 85−92.

Stefanini, S., Desideri, A., Vecchini, P., Drakenberg, T., & Chiancone, E. (1989) *Biochemistry 28*, 378−382.

Styring, S. A., & Rutherford, A. W. (1988) *Biochemistry 27*, 4915−4923.

Sun, S., & Chasteen, N. D. (1992) *J. Biol. Chem. 267*, 25160−25166.

Sun, S., Arosio, P., Levi, S., & Chasteen, N. D. (1993) *Biochemistry 32*, 9362−9369.

Theil, E. C. (1987) *Annu. Rev. Biochem. 56*, 289−315.

Theil, E. C. (1989) *Adv. Enzymol. Relat. Areas Mol. Biol. 63*, 421−449.

Treffry, A., & Harrison, P. M. (1984) *J. Inorg. Chem. 21*, 9−20.

Treffry, A., Bauminger, E. R., Hechel, D., Hodson, N. W., Nowik, I., Yewdall, S. J., & Harrison, P. M. (1993) *Biochem. J. 296*, 721−728.

Waldo, G. S., & Theil, E. C. (1993) *Biochemistry 32*, 13262−13269.

Waldo, G. S., Ling, J., Sanders-Loehr, J., & Theil, E. C. (1993) *Science 259*, 796−798.

Wardeska, J. G., Viglione, B., & Chasteen, N. D. (1986) *J. Biol. Chem. 261*, 6677−6683.

Watt, R. K., Frankel, R. B., & Watt, G. D. (1992) *Biochemistry 31*, 9673−9679.

Xu, B., & Chasteen, N. D. (1991) *J. Biol. Chem. 266*, 19965−19970.

Yang, C., Meagher, A., Huynh, B. H., Sayers, D. E., & Theil, E. C. (1987) *Biochemistry 26*, 497−503.